IJMCM

Babol University
Of Medical Sciences

ORIGINAL ARTICLE

Integrated Bioinformatics and Experimental Validation of the hsa_circ_0000378/miR-205-5p/RAD51 ceRNA Axis in Breast Cancer

Ali Abbasi[1,2] (iD), Nahid Nafisi[3] (iD), Pejman Morovat[4] (iD) , Mitra Nourbakhsh[5] (iD), Mehdi Sepidarkish[6] (iD) , Mohamadreza Ahmadifard[7] (iD) , Arash M. Ashrafi [8] (iD), Mehdi Pouramir[1,8]* (iD)

1. Student Research Committee, Babol University of Medical Sciences, Babol, Iran.
2. Department of Medical Biochemistry, Faculty of Medicine, Babol University of Medical Sciences, Babol, Iran.
3. Surgery Department, Rasoul Akram Hospital Clinical Research Development Center (RCRDC), Iran University of Medical Sciences, Tehran, Iran.
4. Department of Medical Biotechnology, Faculty of Medicine, Babol University of Medical Sciences, Babol, Iran.
5. Department of Biochemistry, Faculty of Medicine, Iran University of Medical Sciences, Tehran, Iran.
6. Department of Biostatistics and Epidemiology, School of Public Health, Babol University of Medical Sciences, Babol, Iran.
7. Department of Medical Genetics and Molecular Biology, Faculty of Medicine, Babol University of Medical Sciences, Babol, Iran.
8. Cellular and Molecular Biology Research Center, Health Research Institute, Babol University of Medical Sciences, Babol, Iran.

ARTICLE INFO	ABSTRACT
	Breast cancer (BC) remains the leading cause of cancer-related mortality in women worldwide, primarily due to its high invasiveness and therapeutic resistance. This study explores the role of noncoding RNAs, circular RNAs (circRNAs), in BC progression through a competing endogenous RNA (ceRNA) network. Three GEO circRNA microarray datasets (GSE101123, GSE165884, GSE182471) were retrieved, normalized, and batch-corrected using ComBat. Differentially expressed circRNAs (DEcircRNAs) were identified via limma ($|\log_2 FC| > 1$, FDR < 0.05). Differentially expressed miRNAs (DEmiRNAs) and mRNAs (DEgenes) were derived from TCGA-BRCA RNA-Seq (1,091 tumors, 113 normals) and miRNA-Seq (1,078 tumors, 104 normals) data using DESeq2 ($|\log_2 FC| > 1$, FDR < 0.05). CircRNAs harboring miRNA response elements (MREs) were selected via CSCD, and miRNA-mRNA interactions predicted through TarBase, prioritizing upregulated DEgenes. A ceRNA network was constructed in Cytoscape based on expression concordance. The hsa_circ_0000378/hsa-miR-205-5p/RAD51 axis was validated in 48 paired BC and adjacent non-tumor tissues by RT-qPCR. Results indicated hsa_circ_0000378 upregulation (2.74-fold, p<0.001), hsa-miR-205-5p downregulation (0.64-fold, p=0.0022), and RAD51 upregulation (3.46-fold, p<0.001) in tumors. Spearman correlations showed negative associations between hsa_circ_0000378 and hsa-miR-205-5p (r = -0.474, p<0.001), hsa-miR-205-5p and RAD51 (r = -0.383, p<0.001), and positive between hsa_circ_0000378 and RAD51 (r = 0.497, p<0.001), supporting ceRNA regulation. ROC analysis revealed RAD51's diagnostic potential (AUC=0.83, 95% CI: 0.74–0.90, sensitivity=0.81, specificity=0.55), followed by hsa_circ_0000378 (AUC=0.75, 95% CI: 0.65–0.85, sensitivity=0.71, specificity=0.77), and hsa-miR-205-5p (AUC=0.66, 95% CI: 0.56–0.76, sensitivity=0.69, specificity=0.55). These results propose the hsa_circ_0000378/hsa_miR-205-5p/RAD51 axis as a potential biomarker; mechanistic validation and larger cohorts are needed for clinical application.

Keywords: Breast Cancer, ceRNA network, Bioinformatic, Circular RNA, Micro RNA, Real-Time PCR, RAD51 |
| *****Corresponding**:
Mehdi Pouramir
Address:
Cellular and Molecular Biology Research Center, Health Research Institute, Babol University of Medical Sciences, Babol, Iran
E-mail:
pouramir@yahoo.com | |

Introduction

Breast cancer (BC) is the most prevalent cancer among women worldwide, constituting approximately 25% of all reported cases (1, 2). Therapeutic outcomes and survival rates are strongly related to the stage of the disease in patients (3). Therefore, early detection plays a crucial role in the success of therapeutic methods and the likelihood of more prolonged survival (4). Despite significant advancements in diagnostic tools and methods, tissue biopsy and histopathological analysis remain the gold standard in BC diagnosis (5). However, traditional methods usually diagnose the disease at an advanced stage, leading to limited therapeutic options and reduced survival chances (4, 6). In recent years, an improved understanding of the molecular mechanisms underlying cancer initiation and progression has driven the development of new early diagnosis strategies, thereby enhancing clinical outcomes.

Among different factors involved in BC cancer development, epigenetic alterations with genetic mutations have drawn significant attention to themselves. Noncoding RNAs (ncRNA), once considered nonfunctional transcriptional remnants, are now recognized as key regulators in epigenetic control (7). These RNAs, which don't encode proteins, strongly affect gene expression by changing chromatin structure and operating at the transcriptional and post-transcriptional levels (8, 9). Changed patterns of ncRNA expression have been reported in different cancers, with some acting as oncogenes or tumor suppressors depending on the background (8, 10). Nevertheless, our understanding of their roles in cancer biology is limited, which requires further research.

The competing endogenous RNA (ceRNA) hypothesis suggests a general framework for enhanced comprehension of the interactions among different RNAs such as circular RNAs (circRNAs), long noncoding RNAs (lncRNAs), microRNAs (miRNAs), and messenger RNAs (mRNAs) (11, 12). This regulatory network has been increasingly implicated in cancer development and progression (13, 14). Meanwhile, circRNAs have emerged as a unique class of RNAs, with their covalently closed-loop structure making them highly stable and resistant to exonuclease degradation (15, 16). Although these RNAs were initially categorized as noncoding, it has been noticed that some of them can code for proteins, and previous hypotheses about them require revision (17, 18). Biologically, circRNAs are involved in various cellular functions and may act as miRNA sponges and affect gene expression (19). It has been revealed recently they can also operate as protein synthesis templates. CircRNAs' potential applications in therapeutics and vaccine development have made them more studied (18, 20).

Aberrant expression of circRNAs has been seen in a wide range of cancers, acting as either carcinogens or tumor suppressors depending on the specific cancer and tissue type (21). The expression of circRNAs affects BC, proposing their potential role as biomarkers in diagnosis, prognosis, and putative therapeutic targets (22, 23). For example, reduced expression of circRNA circ_0006220 lessens its probable sponge effect on miRNA hsa-miR-197-5p, and diminishes the expression of the oncogene cadherin 19 (CDH19). This process helps to enhance tumor suppressor function in triple-negative BC (TNBC) (24). Huang et al., in their study showed that elevated expression of the circRNA Ribonuclease P RNA Component H1 (RPPH1) can promote BC progression and metastasis through the RPPH1-miR signaling axis (25). Despite identifying some effective circRNAs, their exact roles in BC are still not fully understood, and further research is required to elucidate the mechanisms involved in the pathogenesis of this illness.

In this study, we aimed to identify novel and functional circRNAs associated with BC through a combination of bioinformatics analyses and experimental findings. Using The Cancer Genome Atlas (TCGA) data, the hsa_circ_0000378/hsa-miR-205-5p/RAD51 regulatory axis was predicted as a candidate network. This finding was subsequently validated through laboratory experiments, suggesting its putative involvement in BC progression.

Methods

Sample Collection

For this study, forty-eight paired tissue samples - including BC tumor tissues and nearby non-cancerous tissues- were obtained from patients who undergone surgery at Mehrgan, Rouhani, Rasoul Akram, and Khatam Al-Anbiya hospitals during the period from February 2023 and December 2024. Ethical clearance was granted by the Ethics Committee of Babol University of Medical Sciences (approval code:

IR.MUBABOL.HRI.REC.1403.326) in accordance with the Decleration of Helsinki. All samples were evaluated by a certified pathologist to confirm the presence of malignant cells in tumor tissues and the absence of malignancy in non-tumor tissues. Tumor cellularity and purity were assessed histopathologically, ensuring that tumor samples contained at least 70% tumor cells, while adjacent non-tumor tissues, collected at least 2 cm from the tumor margins, were verified to be free of malignant cells. Patients with a history of chemotherapy, radiotherapy, metastasis from other malignancies, or recurrent tumors were excluded. To preserve RNA integrity, tissues were immediately submerged in RNA Later Solution (Yekta Tajhiz Azma, Iran) within minutes of resection to minimize degradation. Samples were

incubated at 4 °C overnight to ensure penetration and then stored at −80 °C until subsequent analysis.

Microarray Data Acquisition and Identification of Differentially Expressed circRNAs (DEcircRNAs)

To detect circRNAs with altered expression in BC, we collected three circRNA microarray datasets from the Gene Expression Omnibus (GEO: https://www.ncbi.nlm.nih.gov/geo/) database using the GEOquery package (26) in R (version 4.2.0) (Figure. 1). Two of the datasets were generated using the same microarray platform (Arraystar Human circRNA Microarray V2, platform ID: 074301), in contrast the third used an earlier version (Arraystar Human circRNA Microarray V1, platform ID: Agilent-069978).
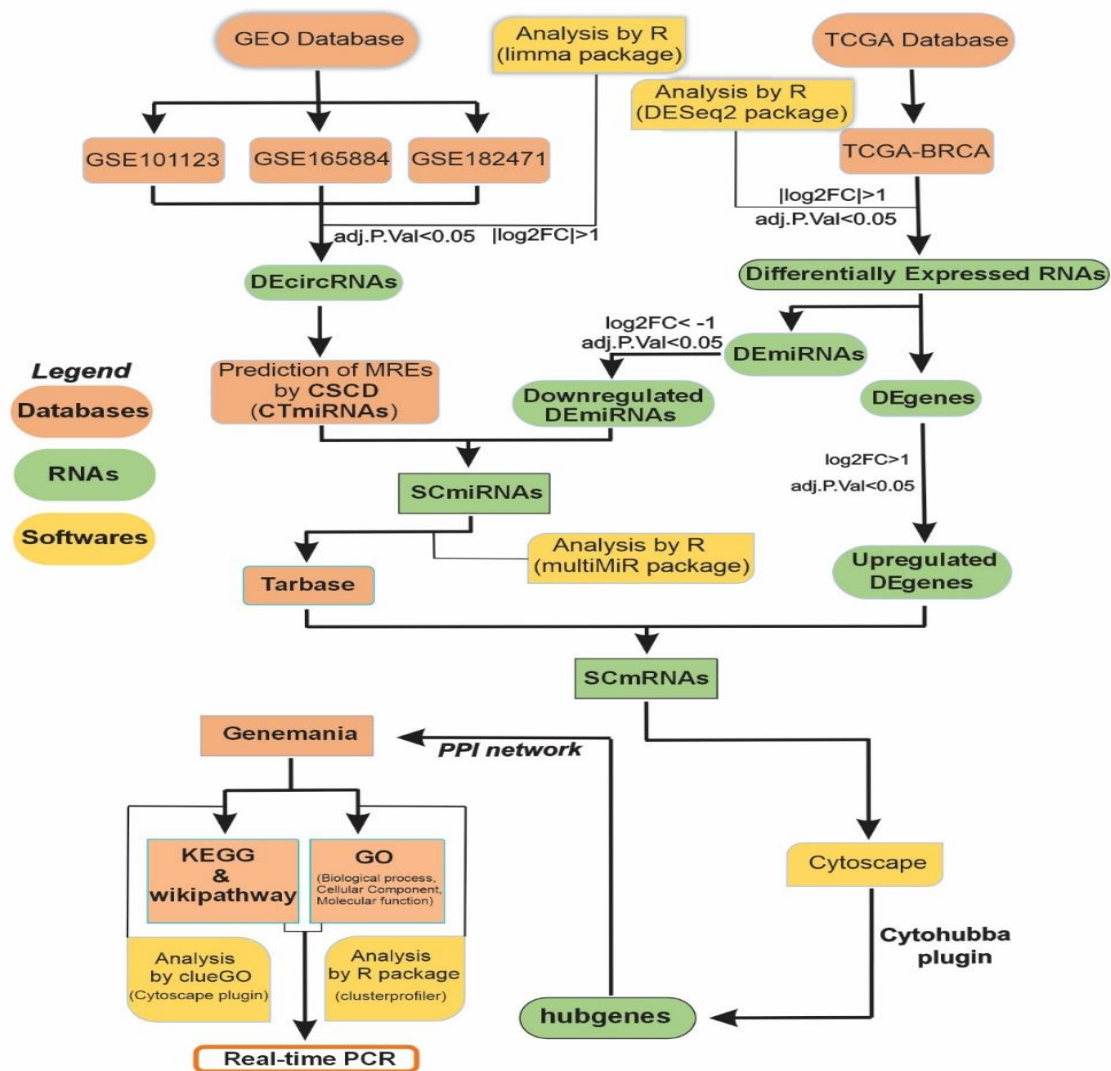

Figure 1. A flowchart illustrating the bioinformatics approaches utilized in this study to identify the final regulatory axis for BC

The collected datasets consisted of: GSE101123: 8 BC samples, three normal breast tissues, GSE165884: 4 BC samples, four adjacent non-tumor tissues, GSE182471: 5 BC samples, five adjacent non-tumor tissues. All raw datasets underwent normalization, and batch-related variations were reduced by applying the Surrogate Variable Analysis (SVA) package (27). Subsequently, differential expression was analyzed using Bioconductor's Linear Models for Microarray (limma) package (28) from Bioconductor, with significance defined as $|\log_2$ Fold change$| > 1$ and adjusted p-value < 0.05.

Identification of Differentially Expressed miRNAs (DEmiRNAs) and mRNAs (DEgenes)

To construct the ceRNA network, TCGA served as the source for both RNA-Seq and miRNA-Seq data, encompassing 1,091 tumors, 113 normal samples for mRNA, and 1,078 tumors, 104 normal samples for miRNA expression. Clinical data were also retrieved from the Genomic Data Commons (GDC) TCGA portal (https://portal.gdc.cancer.gov/). TCGA RNA-seq and miRNA-seq raw counts were downloaded from the GDC portal (accessed on October 10, 2023). Differential expression analysis was performed using the DESeq2 package in R. For visualization and exploratory analysis, counts were normalized using the trimmed mean of M-values (TMM) (29) method implemented in edgeR and transformed with VOOM (limma) (30) through the GDCRNATools (31) package. The DESeq2 package was employed to carry out differential expression analysis (32). Genes and miRNAs with $|\log_2$ Fold change$| > 1$ and adjusted p-value < 0.05 were considered differentially expressed.

Computational forecasting of miRNA Response Elements (MREs)

To predict miRNA binding sites on circRNAs, the Cancer-Specific CircRNA Database (CSCD) (http://gb.whu.edu.cn/CSCD/) (accessed on December 1, 2023) was utilized. This resource was developed based on RNA sequencing data from 87 cancer cell lines and incorporates predictions from four algorithms: CIRI, find_circ, circRNA_finder, and CIRCexplorer, resulting in a comprehensive catalog of 272,152 cancer-related circRNAs. Candidate miRNAs targeting circRNAs-termed CSCD Targeted miRNAs (CTmiRNAs)-were filtered by intersecting them with DEmiRNAs identified from TCGA data. The

overlapping miRNAs were referred to as Shared Consequence miRNAs (SCmiRNAs).

Prediction of miRNA–mRNA Interactions

Target mRNAs of SCmiRNAs were identified using the TarBase database (TarBase v9.0 (accessed on December 5, 2023)) (33) via the multiMiR package (34) in R. Genes overlapping between TarBase-predicted targets and DEgenes from TCGA were defined as Shared Consequence mRNAs (SCmRNAs), representing candidates likely to be involved in BC progression through the ceRNA mechanism.

Constructing the ceRNA Regulatory Network

Using the ceRNA hypothesis as a framework, a circRNA-miRNA-mRNA regulatory network was established. Interactions among DEcircRNAs, SCmiRNAs, and SCmRNAs were integrated and visualized using Cytoscape (https://cytoscape.org/), a widely used platform for biological network analysis.

Detection of Hub Gene and building the Protein-Protein Interaction (PPI) Network

To pinpoint central regulatory genes in the network, the CytoHubba plug-in in Cytoscape was employed which evaluated and ranked nodes through 11 topological algorithms. Additionally, a PPI network was established utilizing data from the STRING database (https://string-db.org/), focusing on proteins encoded by candidate SCmRNAs from the ceRNA network. Interactions with confidence scores of >0.4 were filtered in to focus on high-confidence protein-protein interactions.

Functional Enrichment Analysis of SCmRNAs

Functional annotations of SCmRNAs were explored through Gene Ontology (GO) (35) and Kyoto Encyclopedia of Genes and Genomes (KEGG) (36) analyze, implemented via the ClusterProfiler package (v4.0.2) (37) in R. GO terms were categorized into biological processes (BP), cellular components (CC), and molecular functions (MF). Significance thresholds were established at $p < 0.05$ and $q < 0.05$, applying the Benjamini-Hochberg method for correction (38). For pathway analysis, KEGG was used and visualized using the ClueGO plug-in (39) in Cytoscape. Pathways with adjusted p-value < 0.05 and kappa scores > 0.4 were enriched and biologically meaningful.

Quantitative Polymerase Chain Reaction (qPCR)

Total RNA was extracted using the Kiagene RNA Extraction Kit (Kiagene, Iran), in compliance with the supplier's recommended procedure. The concentration and purity of RNA samples were evaluated with a Nanodrop spectrophotometer (Thermo Fisher Scientific, USA), and integrity was assessed via 1% agarose gel electrophoresis. The Kiagene cDNA Synthesis Kit (Kiagene, Iran) was employed to perform cDNA synthesis with stem-loop primers used for miRNA-specific reverse transcription (40). Divergent primers for hsa_circ_0000378 were designed to span the back splice junction to ensure specific amplification of the circular RNA. Gene expression levels were measured through SYBR Green-based qPCR (Amplicon, Denmark) on the MIC PCR system (Bio Molecular Systems, Australia). Normalization was performed using glyceraldehyde-3-phosphate dehydrogenase (GAPDH) and U6 snRNA as internal controls, and relative expression was determined using the $2^{-\Delta\Delta Ct}$ method. Primer sequences are provided in Table 1.

Statistical Analysis

"Statistical analyses were performed using Stata (v.17 Stata Corp., College Station, TX, USA), GraphPad Prism (v8.0.2), and SPSS (v26). The normality of data distribution was assessed using the Shapiro-Wilk test. Depending on the distribution, comparisons between two groups were made using the Student's t-test (for normally distributed data) or the Mann-Whitney U test (for non-normal data). Correlations between expression levels were determined using Spearman's rank correlation coefficient.

The diagnostic accuracy of each RNA biomarker was evaluated using Receiver Operating Characteristic (ROC) curve analysis. The area under the ROC curve (AUC) and its 95% confidence interval (CI) were calculated using the DeLong method. Internal validation was performed using 2000 bootstrap replicates to calculate bias-corrected AUC values. The optimal cut-off threshold was selected by maximizing Youden's Index (J). At this threshold, sensitivity, specificity, positive predictive value (PPV), and negative predictive value (NPV) were calculated, and their 95% CIs were computed using the Wilson score interval method. A p-value of less than 0.05 was considered statistically significant."

Results

Identification of DEcircRNAs

To explore circRNA expression profiles in BC, three pre-processed microarray datasets were retrieved from the GEO database using the GEOquery package in R. After confirming dataset normalization, they were merged, and the ComBat function within the SVA package was employed to eliminate hidden batch effects (Figure 2). Differential expression analysis using the limma package identified 2,522 circRNAs with significant expression changes. Among them, 40 were defined as DEcircRNAs based on thresholds of adjusted p-value < 0.05 and $|\log_2$ Fold Change$| > 1$. Within this group, 31 genes were upregulated while nine were downregulated in tumor samples compared to normal tissues.

Identification of DEmiRNAs and DEgenes

To construct the ceRNA regulatory network, we analyzed data from the TCGA-BRCA project using DESeq2 in R to identify DEmiRNAs and DEgenes. Applying thresholds of adjusted p-value < 0.05 and $|\log_2$ FC$| > 1$, we identified 96 upregulated and 73 downregulated DEmiRNAs, as well as 1,780 upregulated and 1,296 downregulated DEgenes. Volcano plots illustrating the differential expression of circRNAs, miRNAs, and mRNAs are presented in Figure 3, with upregulated genes shown in red, downregulated in blue, and non-significant genes in black

Prediction of MREs and miRNA–mRNA Interactions

All identified DEcircRNAs were found to harbor MREs, indicating their potential to act as miRNA sponges (Figure. 4). The CSCD database was used to identify miRNAs targeting the CTmiRNAs. These were then intersected with downregulated DEmiRNAs from the TCGA-BRCA dataset, resulting in a group of four miRNAs, termed SCmiRNAs: hsa-miR-205-5p, hsa-miR-335-5p, hsa-miR-483-5p, and hsa-miR-511-5p (Figure. 5A).

The potential target genes of SCmiRNAs were subsequently predicted using the TarBase database through the multiMiR R package (supplementary file 1). These predicted target mRNAs were intersected with upregulated DEgenes derived from TCGA,

identifying 310 shared SCmRNAs as the third axis of the ceRNA network (Figure. 5B)

Construction of the ceRNA Network

Based on the ceRNA hypothesis-whereby circRNAs suppress miRNAs and thereby upregulate target mRNAs-two subnetworks were constructed using Cytoscape: (1) DEcircRNA–SCmiRNA and (2) SCmiRNA-SCmRNA interaction maps, forming the basis of the integrated circRNA-miRNA-mRNA regulatory network.

Hub Gene Identification and PPI Analysis

Key regulatory genes, or hub genes, were detected using the CytoHubba plugin in Cytoscape by applying the Maximal Clique Centrality (MCC) algorithm to rank gene importance. Based on this analysis, the top-ranking hub genes included Ubiquitin Conjugating Enzyme E2 C (**UBE2C**), Kinesin Family Member 4A (**KIF4A**), **Cyclin B2 (CCNB2)**, *Exonuclease 1* (**EXO1**), ERCC Excision Repair 6 Like (**ERCC6L**), Rac GTPase Activating Protein 1 (**RACGAP1**), GINS Complex Subunit 1 (**GINS1**), Karyopherin Subunit Alpha 2 (**KPNA2**), **RAD51**, and *PICALM interacting mitotic regulator* (**PIMREG**) (Figure. 6).

The protein interaction landscape of RAD51 was investigated using the GeneMANIA plug-in within Cytoscape (Figure. 7). In the constructed PPI network, edge colors represent different categories of functional associations, and edge weights are assigned based on the confidence scores provided by the underlying databases. Nodes within the network were interconnected through multiple forms of interactions, including physical interactions (77.64%), co-expression (8.01%), predicted associations (5.37%), co-localization (3.63%), genetic interactions (2.87%), pathway associations (1.88%), and shared protein domains (0.60%). These interaction types collectively accounted for 100% of the network's weighting, reflecting the integrative approach to evaluating the functional relevance of the connected genes. Each pair of interacting genes was scored according to the strength and frequency of paths linking a particular node to the query node. The PPI network analysis of RAD51 revealed its interaction with proteins involved in DNA repair and genomic stability, supporting its known functional role in homologous recombination and maintenance of genome integrity.

The protein interaction landscape of RAD51 was investigated using the GeneMANIA plug-in within Cytoscape (Figure. 7).

In the constructed PPI network, edge colors represent different categories of functional associations, and edge weights are assigned based on the confidence scores provided by the underlying databases. Nodes within the network were interconnected through multiple forms of interactions, including physical interactions (77.64%), co-expression (8.01%), predicted associations (5.37%), co-localization (3.63%), genetic interactions (2.87%), pathway associations (1.88%), and shared protein domains (0.60%).

Table 1. Sequence of primers

| Gene	Primer Type	Primer Sequence	Length (nt)
RAD51	Forward	5'-GCGAGTAGAGAAGTGGAGCG-3'	20
RAD51	Reverse	5'-CAAGCTGCATCTGCATTGCC-3'	20
miR205-5p	Forward	5'-AACACGCTCCTTCATTCCAC-3'	20
miR205-5p	Reverse	5'-GTCGTATCCAGTGCAGGGT-3'	19
Circ-0000378	Forward	5'-TAGATCCTTCAAGTGGCGGC-3'	22
Circ-0000378	Reverse	5'-CTTCGCTGACATCACTCCAG-3'	20
RNU6	Forward	5'-GCTTCGGCAGCACATATACTAAAT-3'	24
RNU6	Reverse	5'-CGCTTCACGAATTTGCGTGTCAT-3'	23
GAPDH	Forward	5'-GAAGGTGAAGGTCGGAGT-3'	18
GAPDH **RT Primer (stem-loop) for miR205-5p**	Reverse	5'-GAAGATGGTGATGGGATTTC-3' 5'-GTCGTATCCAGTGCAGGGTCCGAGGTATTCGCACTGGATACGACCAGACT-3'	20 50
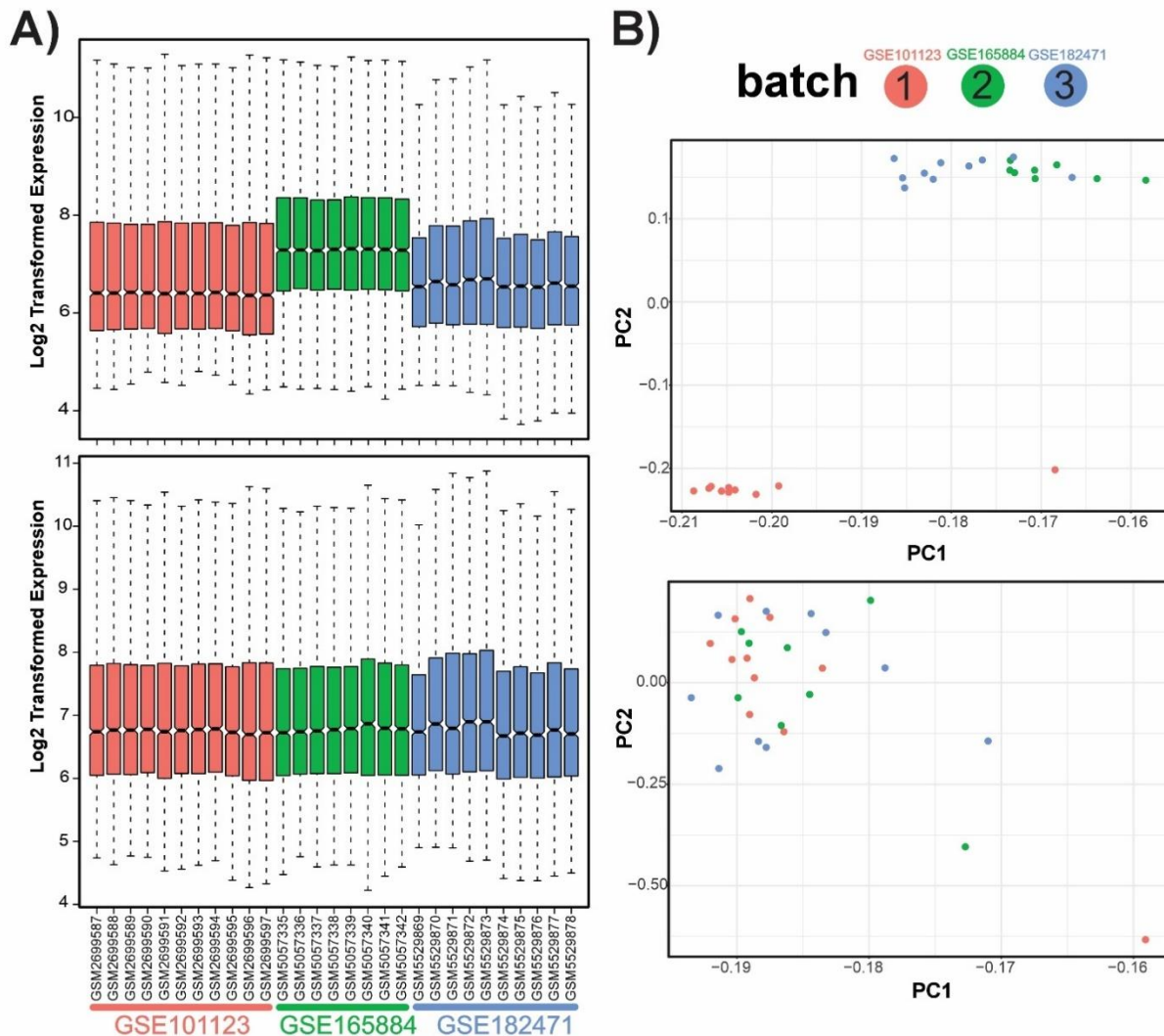
Figure 2. Gene expression patterns from three Arraystar microarrays are illustrated through the box plots: (A) Before batch correction (merged datasets) and (B) after batch effect elimination using the ComBat algorithm implemented in the SVA package in R.

These interaction types collectively accounted for 100% of the network's weighting, reflecting the integrative approach to evaluating the functional relevance of the connected genes. Each pair of interacting genes was scored according to the strength and frequency of paths linking a particular node to the query node. The PPI network analysis of RAD51 revealed its interaction with proteins involved in DNA repair and genomic stability, supporting its known functional role in homologous recombination and maintenance of genome integrity.

These interaction types collectively accounted for 100% of the network's weighting, reflecting the integrative approach to evaluating the functional relevance of the connected genes. Each pair of interacting genes was scored according to the strength and frequency of paths linking a particular node to the

query node. The PPI network analysis of RAD51 revealed its interaction with proteins involved in DNA repair and genomic stability, supporting its known functional role in homologous recombination and maintenance of genome integrity.

The protein interaction landscape of RAD51 was investigated using the GeneMANIA plug-in within Cytoscape (Figure. 7). In the constructed PPI network, edge colors represent different categories of functional associations, and edge weights are assigned based on the confidence scores provided by the underlying databases. Nodes within the network were interconnected through multiple forms of interactions, including physical interactions (77.64%), co-expression (8.01%), predicted associations (5.37%), co-localization (3.63%), genetic interactions (2.87%), pathway associations (1.88%), and shared protein domains (0.60%). These interaction types collectively

accounted for 100% of the network's weighting, reflecting the integrative approach to evaluating the functional relevance of the connected genes. Each pair of interacting genes was scored according to the strength and frequency of paths linking a particular

node to the query node. The PPI network analysis of RAD51 revealed its interaction with proteins involved in DNA repair and genomic stability, supporting its known functional role in homologous recombination and maintenance of genome integrity.
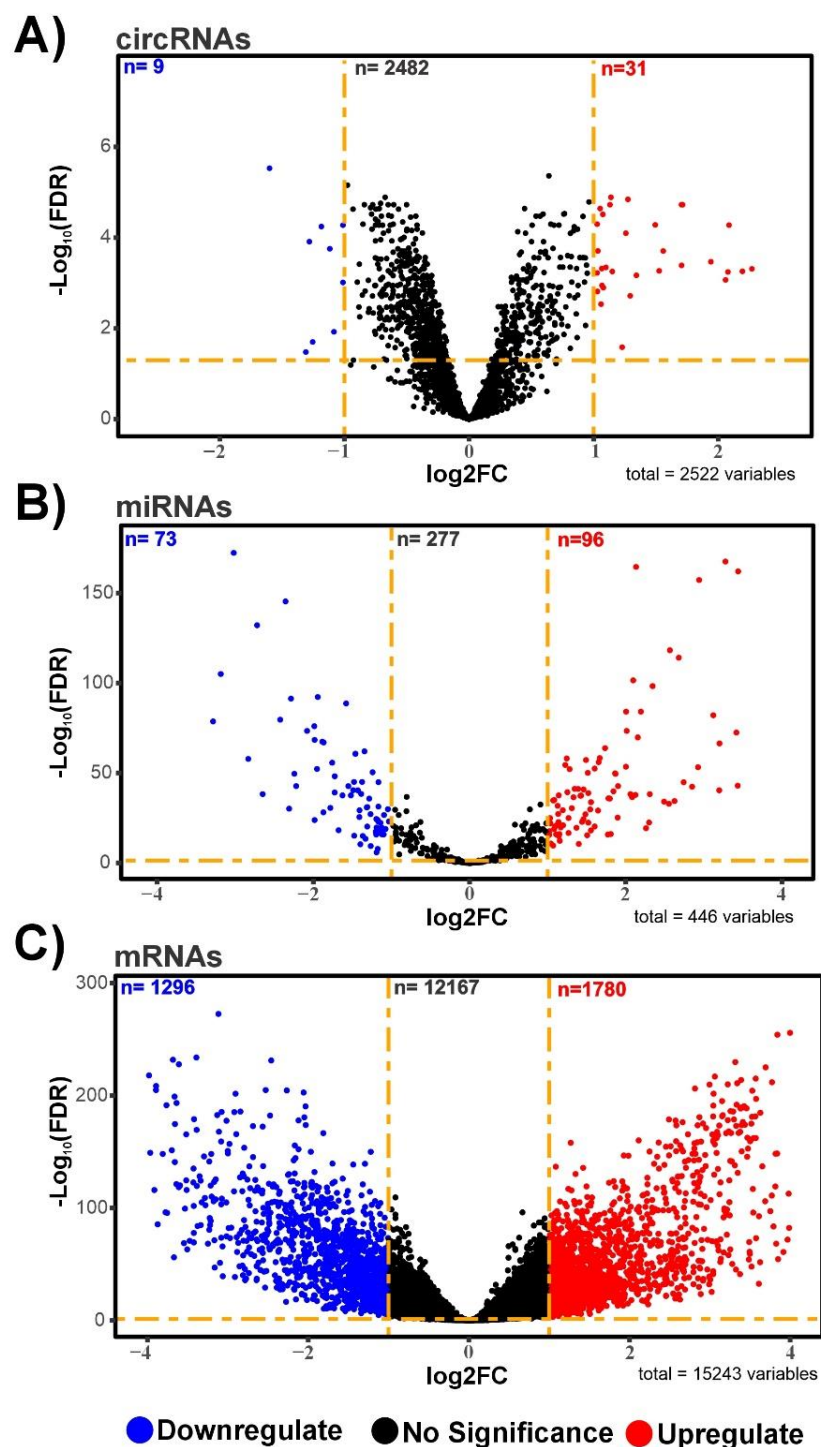

Figure 3. Volcano plots depicting (A) differentially expressed circRNAs (DEcircRNAs) (31 up/9 down DEcircRNAs), (B) differentially expressed miRNAs (DEmiRNAs) (96 up/73 down DEmiRNAs), and (C) differentially expressed mRNAs (DEgenes) (1780 up/1296 down DEgenes). In each plot, blue and red dots represent the downregulated and upregulated transcripts, respectively. The plots were generated using the "EnhancedVolcano" package in R.
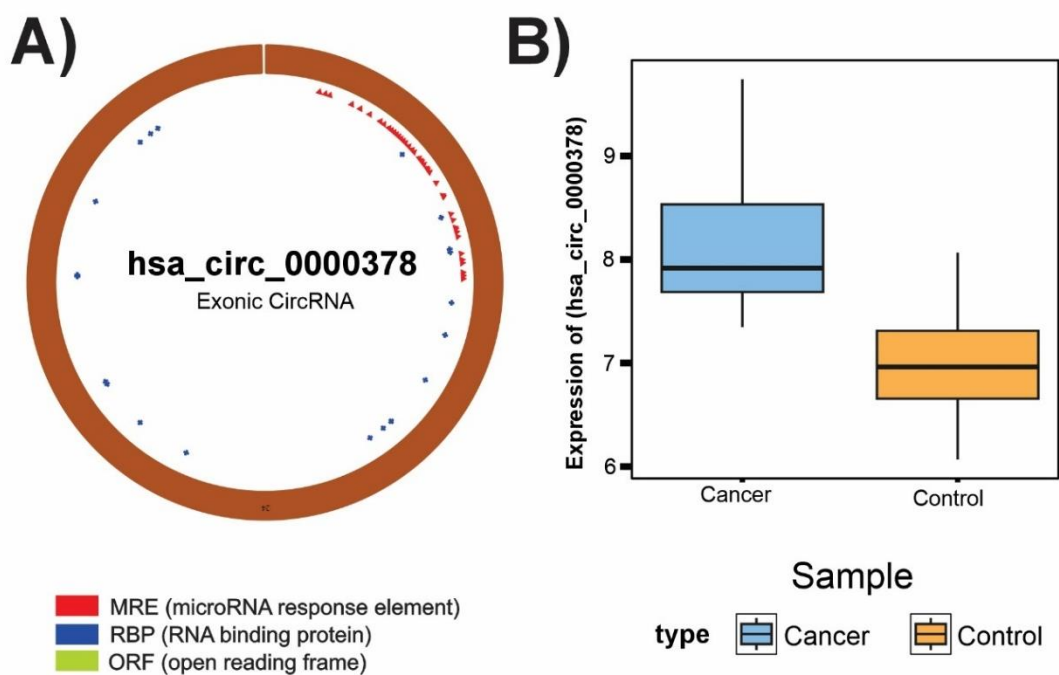
Figure 4. (A) The fundamental structure of differentially expressed circRNA (DEcircRNA), including details on miRNA response elements (MREs), RNA-binding proteins, and open reading frames (ORFs), are illustrated. This schematic representation was obtained from the Cancer-Specific CircRNA Database (CSCD). (B) The expression profile of the DEcircRNA, highlights the differential expression patterns between normal and tumor tissue samples.
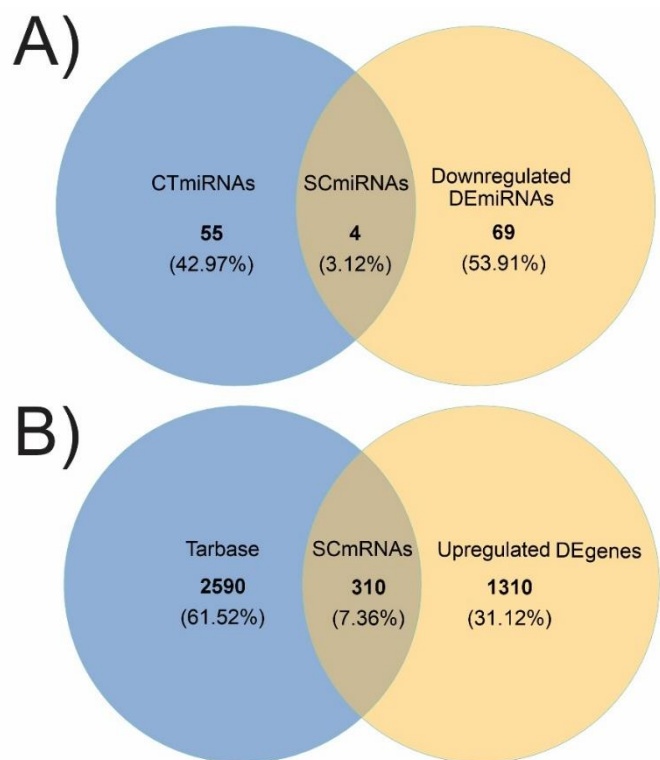

Figure 5. (A) Venn diagram showing the overlap between circRNA-targeted miRNAs (CTmiRNAs, obtained from CSCD) and downregulated differentially expressed miRNAs (DEmiRNAs, obtained from TCGA). The intersection represents shared consequence miRNAs (SCmiRNAs). (B) Venn diagram showing the overlap between TarBase-predicted target genes of SCmiRNAs and upregulated differentially expressed mRNAs (DEgenes, obtained from TCGA). The intersection represents shared consequence mRNAs (SCmRNAs).
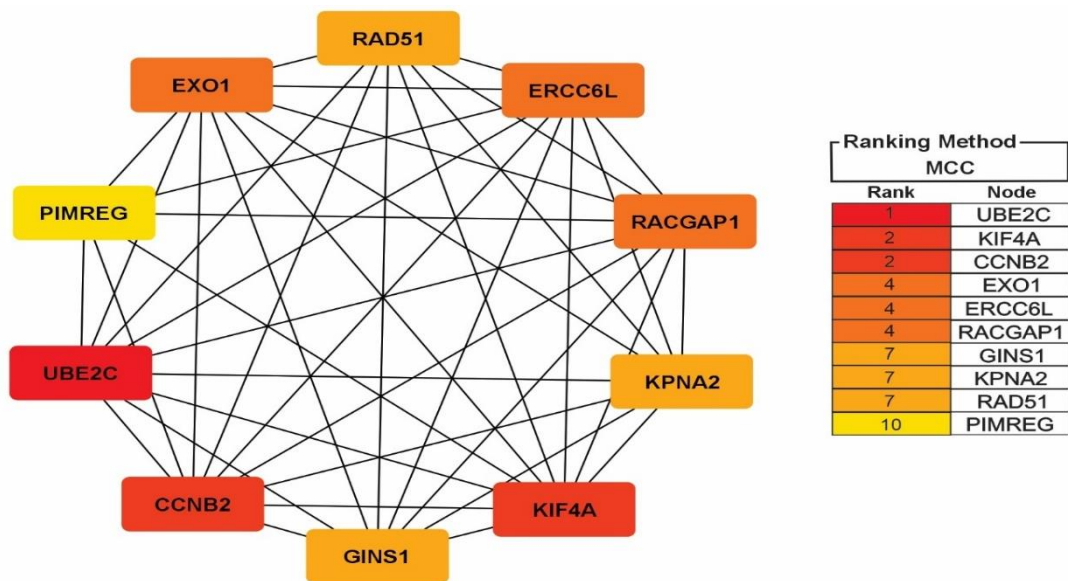
Figure 6. A set of ten central hub genes was identified within the protein-protein interaction (PPI) network. The CytoHubba plug-in in Cytoscape software was employed to rank these genes based on Maximal Clique Centrality (MCC) scores.
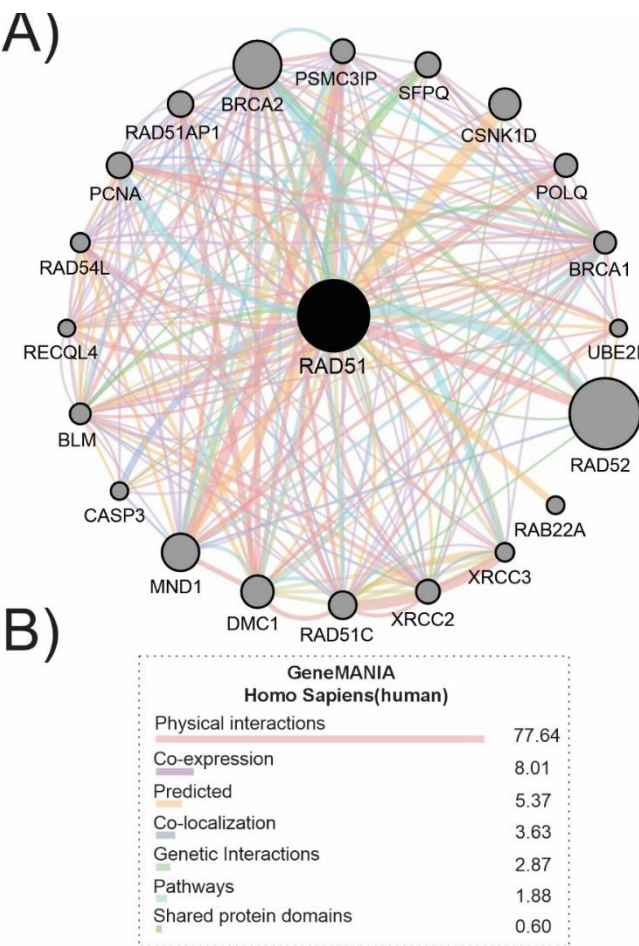

Figure 7. Protein-Protein Interaction (PPI) Network of RAD51. (A) The RAD51-associated PPI network consists of 21 nodes and 210 unique interactions, supported by 495 evidence lines from multiple interaction types. Node size reflects the degree of connectivity, while edge thickness corresponds to the interaction weight assigned by GeneMANIA. (B) Edge colors denote different categories of functional associations, as indicated in the key: pink = physical interactions, purple = co-expression, yellow = predicted associations, blue = co-localization, green = genetic interactions, light blue = pathway associations, and grey = shared protein domain.

Functional Enrichment Analysis

The RAD51 PPI network, comprehensive enrichment analyses were conducted using GO and KEGG databases. GO analysis was categorized into three main domains: BP, CC, and MF. Within the BP category, genes were mainly enriched in pathways including organelle fission, chromosome segregation, and nuclear division, indicating a strong involvement in cell cycle control mechanisms (Figure. 8A). Regarding CC terms, the DEgenes were significantly associated with specific cellular structures including chromosomal region, spindle, and condensed chromosome (Figure. 8B).

In the MF category, a marked enrichment was observed in functions such as tubulin binding, microtubule binding, and catalytic activity, acting on DNA, all of which are essential in controlling replication process (Figure. 8C). To represent these enrichment results visually, a cnetplot was constructed using the clusterProfiler package in R, illustrating the association between individual genes and specific GO or KEGG terms across the BP, CC, MF, and pathway domains (Figure. 8A-C).

To investigate the potential biological roles of the 20 genes identified in the RAD51 PPI network, KEGG pathway enrichment analysis was performed using ClueGO, a plug-in within the Cytoscape platform. The study used a statistical significance threshold of p ≤ 0.05 and a kappa score of ≥ 0.4. The resulting visualizations highlighted interconnected networks of enriched pathway terms. The findings indicated that these 20 genes associated with the RAD51 PPI network are significantly involved in several key biological pathways, including homologous recombination and integrated cancer pathways, suggesting their potential roles in critical cellular and molecular processes (Figure. 8D).

The circRNA *hsa_circ_0000378* was, ultimately, prioritized for further investigation based on its consistent upregulation across multiple GEO datasets (GSE101123, GSE165884, and GSE182471) with $|\log_2 FC| > 1$ and adjusted *p* < 0.05. In addition, it harbors predicted miRNA response elements (MREs) for *hsa-miR-205-5p*, as identified using the CSCD, and exhibits concordant expression with *RAD51*, suggesting a potential role in ceRNA-mediated regulation. Collectively, *hsa_circ_0000378* was selected owing to its significant differential expression in BC tissues, predicted interaction with *hsa-miR-205-*

5p, and correlated expression with *RAD51*, highlighting its potential involvement in BC progression.

aExpression of hsa_circ_0000378, hsa-miR-205-5p, and RAD51 in BC Tissues and Diagnostic Potential

The study cohort consisted of 48 patients, with an average age of 62.6 ± 11.5 years (range: 45-82), reflecting a predominantly middle-aged to elderly population. Anthropometric measurements revealed a mean height of 159.7 ± 5.5 cm, weight of 71.2 ± 10.7 kg, and BMI of 27.7 ± 3.7, indicating that the cohort was vastly overweight (BMI ≥25). Tumor characteristics showed a mean tumor size of 1.7 ± 0.6 cm, with most tumors classified as grade 2 (47.9%) and most patients at stage 2 (52.1%).

Hormone receptor status analysis demonstrated high positivity rates for estrogen receptor (ER, 87.5%) and progesterone receptor (PR, 81.3%), while HER2 overexpression was observed in 27.1% of cases. Lymph node involvement was detected in 45.8% of patients, suggesting a moderate prevalence of regional metastasis. To contextualize the expression and ROC analyses, tumor samples were classified into surrogate immunohistochemistry (IHC)-based subtypes using estrogen receptor (ER), progesterone receptor (PR), and HER2 status, as Ki-67 data were not available. The cohort included 18 (37.5%) Luminal A-like (ER+ and/or PR+, HER2−), 12 (25.0%) Luminal B-like (HER2−, ER+ and/or PR+), 12 (25.0%) Luminal B-like (HER2+, ER+ and/or PR+), 1 (2.1%) HER2-enriched (ER−, PR−, HER2+), and 5 (10.4%) Triple-negative (ER−, PR−, HER2−) cases (Table 2).

Changes in the expression of genes in the hsa_circ_0000378/hsa-miR-205-5p/RAD51 axis were analyzed in 48 paired BC tissues and adjacent non-tumor tissues using r*everse transcription-quantitative polymerase chain reactio*n (RT-qPCR). The results revealed that the expression of hsa_circ_0000378 was significantly higher in BC tumor tissues compared to non-tumor tissues (2.74-fold, p<0.001) (Figure. 9A). analysis of hsa-miR-205-5p expression showed that, in contrast to hsa_circ_0000378, its expression was significantly reduced in BC tumor tissues compared to non-tumor tissues (0.64-fold, p=0.0022) (Figure. 9B). The expression of RAD51 showed the greatest increase among the genes analyzed, being 3.46-fold higher in tumor tissues compared to non-tumor tissues (p<0.001) (Figure. 9C) (supplementary file 2).
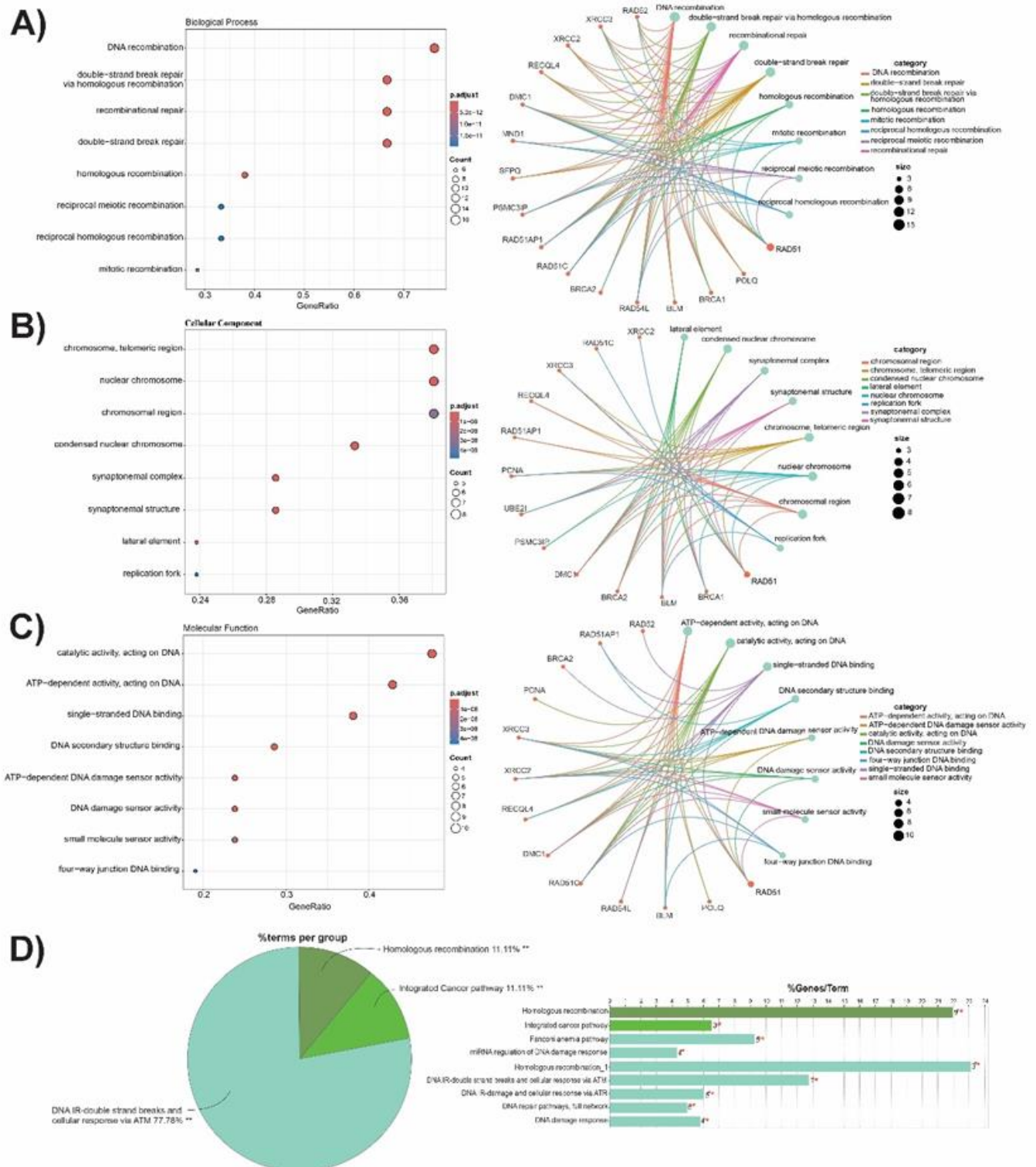
Figure 8. Dot Plot and Cnetplot Representing Gene Ontology (GO) term, including (A) biological process (BP), (B) cellular component (CC), and (C) molecular function (MF). Terms positioned higher in the plots are more statistically significant than those lower down. The cnetplots illustrate the relationships between specific proteins from PPI network of RAD51 and enriched GO terms in the categories of (A) BP, (B) CC, and (C) MF. The RAD51 gene is highlighted in bold for emphasis. In KEGG Pathway Analysis (D), The bar graph illustrates the number of genes identified for each KEGG pathway. The percentages displayed above the bars represent the proportion of detected genes compared to the total number of genes associated with each term. The pie chart provides a general overview of the functional categories of PPI network of RAD51, with each group labeled according to the most significantly enriched term. The bar graph and the pie chart were generated using ClueGO, a plugin within the Cytoscape platform.

Table 2. Demographic and Clinical Characteristics of Patients

Characteristic	Value (Mean ± SD or n (%))	Range
Age (years)	62.6 ± 11.5	45–82
Height (cm)	159.7 ± 5.5	148–173
Weight (kg)	71.2 ± 10.7	48.6–100
BMI	27.7 ± 3.7	19.5–36.8
Tumor size (cm)	1.7 ± 0.6	1–3
Tumor stage		
Stage 1	13 (27.1%)	
Stage 2	25 (52.1%)	
Stage 3	7 (14.6%)	
Stage 4	3 (6.2%)	
Tumor grade		
Grade 1	7 (14.6%)	
Grade 2	23 (47.9%)	
Grade 3	18 (37.5%)	
Tumor type		
Type 1 (IDC*)	39 (81.3%)	
Type 2 (Other)	9 (18.7%)	
Tumor necrosis		
Present	9 (18.8%)	
Absent	15 (31.3%)	
Not identified	24 (49.9%)	
Perineural Invasion		
Present	4 (8.3%)	
Absent	28 (58.3%)	
Not identified	16 (33.4%)	
ER receptor		
Positive	42 (87.5%)	
Negative	6 (12.5%)	
PR receptor		
Positive	39 (81.3%)	
Negative	9 (18.7%)	
HER2 status		
Positive	13 (27.1%)	
Negative	35 (72.9%)	
Lymph node involvement		
Yes	22 (45.8%)	
No	26 (54.2%)	
Surrogate IHC Subtype Luminal A-like	18 (37.5%)	

Characteristic	Value (Mean ± SD or n (%))	Range
Luminal B-like (HER2-)	12 (25%)	
Luminal B-like (HER2+)	12 (25%)	
HER-enriched	1 (2.1%)	
Triple-negative	5 (10.4%)	

*IDC: Invasive Ductal Carcinoma, HER2: Human Epidermal growth factor Receptor 2, PR: Prolactin Receptor, ER: Esterogen Receptor, IHC:Immunohistochemistry
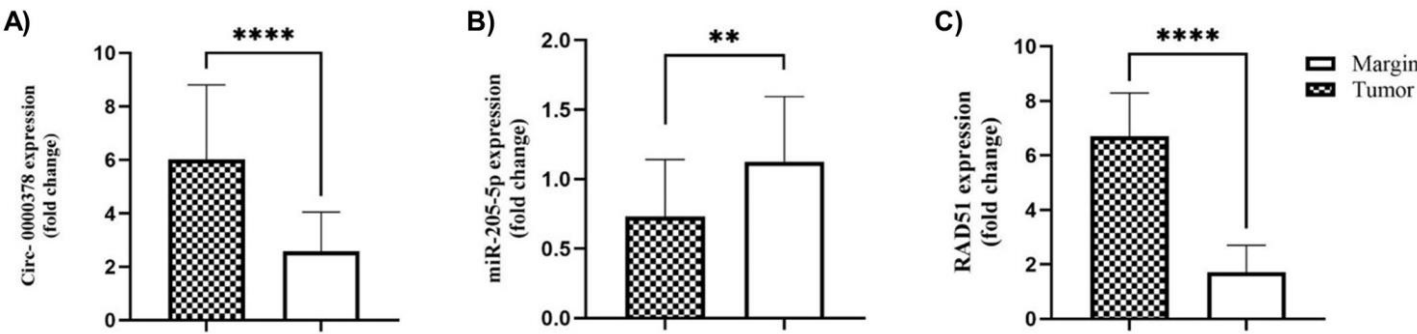

Figure 9. Analysis of hsa_circ_0000378/hsa-miR-205-5p/RAD51 axis expression in BC tissues. The relative expression of hsa_circ_0000378 (A), hsa-miR-205-5p (B), and RAD51 mRNA (C) in 48 BC tissues versus adjacent non-tumor tissues was evaluated using RT-qPCR. **p < 0.01 and ****p < 0.0001.

To evaluate the proposed regulatory relationship within the hsa_circ_0000378/hsa-miR-205-5p/RAD51 axis, we performed Spearman correlation analysis on the expression levels of these three molecules across all tissue samples. The results revealed a statistically significant negative correlation between the expression of hsa_circ_0000378 and hsa-miR-205-5p (r = -0.474, p < 0.001). Furthermore, hsa-miR-205-5p expression showed a significant negative correlation with its putative target, RAD51 (r = -0.383, p < 0.001). Concordantly, a significant positive correlation was observed between the expression of hsa_circ_0000378 and RAD51 (r = 0.497, p < 0.001). This expression pattern-an inverse circRNA-miRNA correlation, an inverse miRNA-mRNA correlation, and a positive circRNA-mRNA correlation-is consistent with the core principle of the ceRNA hypothesis and supports the proposed model in which hsa_circ_0000378 may acts as a sponge for hsa-miR-205-5p, thereby alleviating its repression of RAD51.

The circRNA hsa_circ_0000378 exhibited moderate diagnostic performance, with an Area Under the Curve (AUC) of 0.75 (95% CI: 0.65–0.85). At an optimal threshold of 2.30 (95% CI: 1.85–2.76), it achieved a sensitivity of 0.71 (95% CI: 0.56–0.83) and specificity of 0.77 (95% CI: 0.62–0.88) (Figure. 10A). This performance suggests that hsa_circ_0000378 contributes to BC-related regulatory networks, though its variable AUC indicates heterogeneity in its functional impact across patients. In contrast, hsa-miR-205-5p demonstrated the lowest diagnostic accuracy, with an AUC of 0.66 (95% CI: 0.56–0.76). At its optimal threshold of 0.64 (95% CI: 0.13–1.16), it yielded a sensitivity of 0.69 (95% CI: 0.54–0.81) and specificity of 0.55 (95% CI: 0.40–0.69) (Figure. 10B).

The lower AUC reflects its limited direct role in BC biology, likely due to its context-dependent function within complex regulatory networks. Conversely, RAD51 showed the highest diagnostic capacity, with an AUC of 0.83 (95% CI: 0.74–0.90). At its optimal threshold of 1.68 (95% CI: 0.57–2.72), it achieved a sensitivity of 0.81 (95% CI: 0.67–0.91) and specificity of 0.55 (95% CI: 0.40–0.70) (Figure. 10C).

Despite comparable sensitivity and specificity across these molecules, RAD51's elevated AUC underscores its critical role in BC molecular mechanisms, particularly in DNA repair pathways (Table 3).
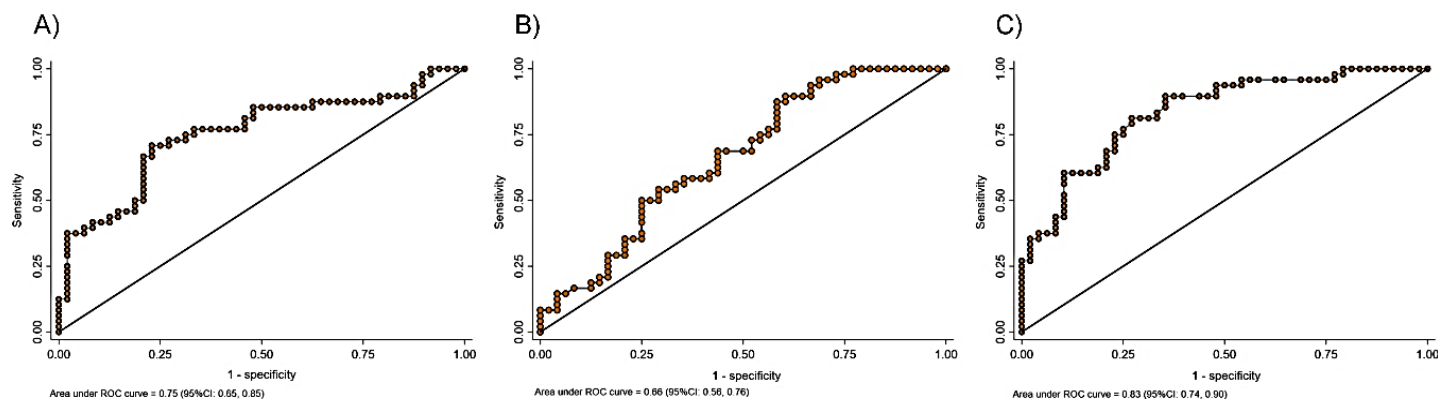
Figure 10. ROC curve analysis of hsa_circ_0000378 (A), hsa-miR-205-5p (B) RAD51 (C). AUC: Area Under the Curve, NPV: Negative Predictive Value, PPV: Positive Predictive Value

Table 3. Diagnostic indices for each evaluated RNA in identifying BC

Variables	AUC (95% CI)	Best threshold	Specificity (95% CI)	Sensitivity (95% CI)	PPV (95% CI)	NPV (95%CI)
hsa_circ_0000378	0.75 (0.65, 0.85)	2.30 (1.85, 2.76)	0.77 (0.63, 0.88)	0.71 (0.56, 0.83)	0.76 (0.61, 0.87)	0.73 (0.58, 0.84)
RAD51	0.83 (0.74, 0.90)	1.68 (0.57, 2.72)	0.55 (0.40, 0.70)	0.81 (0.67, 0.91)	0.75 (0.61, 0.86)	0.79 (0.64, 0.90)
hsa-miR-205-5p	0.66 (0.56, 0.76)	0.64 (0.13, 1.16)	0.55 (0.41, 0.70)	0.69 (0.54, 0.81)	0.61 (0.47, 0.74)	0.63 (0.47, 0.78)

AUC: Area Under the Curve, NPV: Negative Predictive Value, PPV: Positive Predictive Value

Discussion

As one of the most common cancers in women, BC leads to significant mortality worldwide, because of its high prevalence and issues related to tumor invasion and metastasis. Despite significant advancements in treatment strategies, the poor prognosis of BC in advanced cases highlights the necessity of investigating the underlying biological mechanisms driving disease progression. Gaining insight into these mechanisms is crucial for discovering new diagnostic markers and treatment candidates. (41). In the present study, through integrative bioinformatics analysis, we identified a ceRNA regulatory axis involving hsa_circ_0000378, hsa-miR-205-5p, and RAD51, which may represent a candidate pathway with a putative role in BC progression. Our findings show that hsa_circ_0000378 expression is elevated in BC tumor tissues compared to adjacent non-tumor tissues. We propose that this molecule may act as a sponge for hsa-miR-205-5p, reducing its inhibitory effect on RAD51 mRNA, thereby leading to increased RAD51 levels, which might enhance DNA repair in cancer cells and contribute to tumor survival (42).

To elucidate the regulatory relationships within the hsa_circ_0000378/hsa-miR-205-5p/RAD51 axis, we conducted Spearman correlation analysis, as detailed in the Results section. The analysis revealed a marked negative correlation between hsa_circ_0000378 and hsa-miR-205-5p (r = -0.474, p < 0.001), indicating that higher hsa_circ_0000378 expression is associated with reduced hsa-miR-205-5p levels, consistent

with the ceRNA hypothesis. Additionally, a negative correlation was observed between hsa-miR-205-5p and RAD51 (r = -0.383, p < 0.001), suggesting that decreased miRNA levels alleviate RAD51 suppression. Concordantly, a positive correlation was found between hsa_circ_0000378 and RAD51 (r = 0.497, p < 0.001), supporting the hypothesis that hsa_circ_0000378 promotes RAD51 expression by sequestering hsa-miR-205-5p. These patterns align with the ceRNA regulatory model, providing robust evidence for this axis in BC progression.

CircRNAs, due to their covalently closed-loop structure and resistance to exonuclease degradation, are key regulators in cancer biology, influencing gene expression at transcriptional and post-transcriptional levels. They may act as miRNA sponges, regulate mRNA translation, or encode functional peptides, playing pivotal roles in tumorigenesis (43, 44). Numerous studies have confirmed the differential expression of circRNAs in BC, underscoring their pivotal role in tumorigenesis and disease progression (45). In BC, circRNAs such as circBCBM1 show marked overexpression in plasma, positioning them as promising non-invasive diagnostic biomarkers (46). Similarly, hsa_circ_0001785 demonstrates superior diagnostic accuracy compared to CEA and CA15-3, highlighting its potential as a novel diagnostic tool (47). Stability and diverse regulatory roles make them promising candidates for cancer biomarker development (48, 49).

The hsa-miR-205-5p molecule has been studied in various cancers, including breast, colorectal, liver, and lung cancer(50-53). It acts as a tumor suppressor in BC and prostate cancer by targeting genes like PTEN, ZEB1, and E-cadherin to inhibit proliferation, motility, and epithelial-mesenchymal transition (EMT) (54-57), while functioning as an oncogene in lung and liver cancers by promoting cell proliferation and survival (52, 53). This functional duality is rooted in the complex interactions of hsa-miR-205-5p with a set of mRNA targets in different tissues (58). The role of hsa-miR-205-5p is highly context-dependent, varying across BC subtypes (e.g., Luminal vs. Triple-negative) and tumor types (59). Its context-dependent role is particularly relevant given our cohort's subtype distribution. The surrogate IHC-based classification, incorporating ER, PR, and HER2 status, showed a predominance of Luminal A-like (37.5%) and Luminal B-like (50.0%) tumors, aligning with high ER+ and PR+ rates. However, the upregulation of hsa_circ_0000378 and RAD51, alongside hsa-miR-205-5p downregulation, may have greater functional significance in Triple-negative and HER2-enriched subtypes, where DNA repair pathways, particularly homologous recombination, are critical for tumor survival (60). In addition to its functional roles, hsa-miR-205-5p shows potential as a biomarker for cancer diagnosis and progression prediction (61). It also holds significant potential from the perspective of RNA-based therapies. However, for full utilization of its therapeutic potential, more extensive studies are required to identify its exact molecular mechanisms and assess its effectiveness in clinical settings.

As a crucial part of the Homologous Recombination pathway, RAD51 repairs DNA double-strand breaks, protects against genetic damage, and ensures genomic stability (62, 63). It plays a protective role in healthy tissues, but in cancer cells, its overexpression is associated with tumor progression and resistance to therapy (60, 62). In BC cells with BRCA1/2 mutations, the homologous recombination pathway is compromised, making these cells dependent on RAD51 for survival (64). Increased levels of RAD51 have been associated with advanced tumor grade and stage, larger tumor size, and greater resistance to chemotherapy in BC (65-67).

Overexpression of RAD51 increases resistance to DNA-damaging therapies like Poly (ADP-ribose) polymerase inhibitors and is associated with a worse prognosis, especially in TNBC subtypes (64). In line with previous reports, our study confirmed that RAD51 alone exhibits strong diagnostic performance (AUC = 0.83); however, its limited specificity (0.55) reflects the inherent heterogeneity of BC and underscores the need for multi-marker approaches to enhance patient stratification. In this study, we identified hsa_circ_0000378 as a novel circRNA in BC, previously uncharacterized in this or other cancer types. Our data suggest that

hsa_circ_0000378 participates in a regulatory ceRNA axis with hsa-miR-205-5p and RAD51. The observed downregulation of hsa-miR-205-5p, consistent with its tumor-suppressive function, combined with its interaction with hsa_circ_0000378, provides a plausible mechanism for RAD51 upregulation in tumor tissues. The potential utility of hsa_circ_0000378 lies not in replacing RAD51, but in its possible role as an upstream regulatory biomarker that may provide mechanistic insight into the epigenetic regulation of homologous recombination proficiency in specific tumor subsets. While RAD51 may reflect downstream functional consequences, hsa_circ_0000378 could represent an initiating regulatory event.

We propose that a combined biomarker signature integrating hsa_circ_0000378 and RAD51 might offer improved diagnostic and prognostic performance compared to either marker alone, potentially enhancing sensitivity and accuracy for identifying patients with this specific subtype of homologous recombination spathogenesis highlights its novelty and potential importance. Nevertheless, to fully substantiate its biological and clinical significance, further in vitro and in vivo studies are required. Future investigations should aim to elucidate the precise molecular mechanisms through which this axis influences tumor biology, including its impact on cell proliferation, invasion, and therapy resistance, thereby validating its potential as a candidate biomarker and therapeutic target. The absence of Ki-67 data limited the precision of surrogate IHC-based subtyping, and future studies incorporating Ki-67 and PAM50 profiling are recommended to refine subtype-specific analyses.

The current study has certain limitations that warrant attention in future research. Notably, the sample size (n=48) was relatively small, and the AUC values derived from this tissue-based cohort are preliminary, limiting their generalizability. To address this, validation in larger, independent, and preferably prospective cohorts is essential to confirm the diagnostic potential of the identified axis. Furthermore, evaluating the expression of hsa_circ_0000378, hsa-miR-205-5p, and RAD51 in accessible biofluids, such as plasma or serum, is critical to assess their feasibility as non-invasive

biomarkers, which would significantly enhance their clinical utility.

In conclusion, we propose the hsa_circ_0000378/hsa-miR-205-5p/RAD51 axis as a promising regulatory network in BC, supported by robust bioinformatics predictions and expression analysis in patient tissues. To establish causality and evaluate its translational potential, the following immediate next steps are recommended: (i) mechanistic studies, including AGO2-RIP, luciferase reporter assays, and perturbation/rescue experiments, to confirm direct circRNA–miRNA interactions and their functional effects on RAD51 expression; (ii) protein-level analyses and functional assessments of DNA repair pathways to elucidate RAD51's role in tumor survival; and (iii) validation in larger, independent clinical cohorts, incorporating plasma-based studies to explore non-invasive biomarker applications. These efforts will determine whether this axis can serve as a reliable biomarker or, pending rigorous mechanistic validation, a potential therapeutic target, paving the way for improved BC diagnosis and treatment strategies.

Acknowledgment

Funding

References

1. Giaquinto AN, Sung H, Newman LA, et al. Breast cancer statistics 2024. CA Cancer J Clin. 2024;74(6):477-95.
2. Bray F, Laversanne M, Sung H, et al. Global cancer statistics 2022: GLOBOCAN estimates of incidence and mortality worldwide for 36 cancers in 185 countries. CA Cancer J Clin. 2024;74(3):229-63.

3. Antonini M, Mattar A, Pereira TM, et al. Pathologic complete response and breast cancer survival post-neoadjuvant chemotherapy: A systematic review and meta-analysis of real-world data. Heliyon. 2025;11(10).

4. Wang J, Wu SG. Breast Cancer: An Overview of Current Therapeutic Strategies, Challenge, and Perspectives. Breast Cancer. 2023;15:721-30.

5. Zeiser FA, da Costa CA, Roehe AV, et al. Breast cancer intelligent analysis of histopathological data: A systematic review. Adv. Soft Comput. 2021;113:107886.

6. Xiong X, Zheng L-W, Ding Y, et al. Breast cancer: pathogenesis and treatments. Signal Transduct Target Ther. 2025;10(1):49.

7. Wei J-W, Huang K, Yang C, et al. Non-coding RNAs as regulators in epigenetics. Oncol. Rep. 2017;37(1):3-9.

8. Han TS, Hur K, Cho HS, et al. Epigenetic Associations between lncRNA/circRNA and miRNA in Hepatocellular Carcinoma. Cancers (Basel). 2020;12(9):2622.

9. Guz M, Jeleniewicz W, Cybulski M. Interactions between circRNAs and miR-141 in Cancer: From Pathogenesis to Diagnosis and Therapy. Int J Mol Sci. 2023;24(14):11861.

10. Anastasiadou E, Jacob LS, Slack FJ. Non-coding RNA networks in cancer. Nat Rev Cancer. 2018;18(1):5-18.

11. Ala U. Competing Endogenous RNAs, Non-Coding RNAs and Diseases: An Intertwined Story. Cells. 2020;9(7):1574.

12. Tay Y, Rinn J, Pandolfi PP. The multilayered complexity of ceRNA crosstalk and competition. Nature. 2014;505(7483):344-52.

13. Yang N, Liu K, Yang M, et al. ceRNAs in Cancer: Mechanism and Functions in a Comprehensive Regulatory Network. J Oncol. 2021;2021:4279039.

14. Xiong G, Pan S, Jin J, et al. Long Noncoding Competing Endogenous RNA Networks in Pancreatic Cancer. Front Oncol. 2021;11:765216.

15. Fontemaggi G, Turco C, Esposito G, et al. New Molecular Mechanisms and Clinical Impact of circRNAs in Human Cancer. Cancers (Basel). 2021;13(13):3154.

16. Barrett SP, Salzman J. Circular RNAs: analysis, expression and potential functions. Development. 2016;143(11):1838-47.

17. Crudele F, Bianchi N, Terrazzan A, et al. Circular RNAs Could Encode Unique Proteins and Affect Cancer Pathways. Biology (Basel). 2023;12(4):493.

18. Bach DH, Lee SK, Sood AK. Circular RNAs in Cancer. Mol Ther Nucleic Acids. 2019;16:118-29.

19. Zhou WY, Cai ZR, Liu J, et al. Circular RNA: metabolism, functions and interactions with proteins. Mol Cancer. 2020;19(1):172.

20. Bu T, Yang Z, Zhao J, et al. Expanding the Potential of Circular RNA (CircRNA) Vaccines: A Promising Therapeutic Approach. Int J Mol Sci. 2025;26(1):379.

21. Verduci L, Strano S, Yarden Y, et al. The circRNA-microRNA code: emerging implications for cancer diagnosis and treatment. Mol Oncol. 2019;13(4):669-80.

22. Rao A, Arvinden VR, Ramasamy D, et al. Identification of novel dysregulated circular RNAs in early-stage breast cancer. J Cell Mol Med. 2021;25(8):3912-21.

23. Li LX, Hao Y, Dong L, et al. Circular RNAs as Biomarkers in Breast Cancer Diagnosis, Prognosis, Molecular Types, Metastasis and Drug Resistance. Technol Cancer Res Treat. 2025;24:15330338251328500.

24. Shi Y, Han T, Liu C. CircRNA hsa_circ_0006220 acts as a tumor suppressor gene by regulating miR-197-5p/CDH19 in triple-negative breast cancer. Ann Transl Med. 2021;9(15):1236.

25. Huang Y, Zheng W, Ji C, et al. Circular RNA circRPPH1 promotes breast cancer progression via circRPPH1-miR-512-5p-STAT1 axis. Cell Death Discov. 2021;7(1):376.

26. Davis S, Meltzer PS. GEOquery: a bridge between the Gene Expression Omnibus (GEO) and BioConductor. Bioinformatics. 2007;23(14):1846-7.

27. Leek JT, Johnson WE, Parker HS, et al. The sva package for removing batch effects and other unwanted variation in high-throughput experiments. Bioinformatics. 2012;28(6):882-3.

28. Ritchie ME, Phipson B, Wu D, et al. limma powers differential expression analyses for RNA-sequencing and microarray studies. Nucleic Acids Res. 2015;43(7):e47.

29. Robinson MD, Oshlack A. A scaling normalization method for differential expression analysis of RNA-seq data. Genome Biol. 2010;11(3):R25.

30. Law CW, Chen Y, Shi W, et al. voom: Precision weights unlock linear model analysis tools for RNA-seq read counts. Genome Biol. 2014;15(2):R29.

31. Li R, Qu H, Wang S, et al. GDCRNATools: an R/Bioconductor package for integrative analysis of lncRNA, miRNA and mRNA data in GDC. Bioinformatics. 2018;34(14):2515-7.

32. Love MI, Huber W, Anders S. Moderated estimation of fold change and dispersion for RNA-seq data with DESeq2. Genome Biol. 2014;15(12):550.

33. Skoufos G, Kakoulidis P, Tastsoglou S, et al. TarBase-v9.0 extends experimentally supported miRNA-gene interactions to cell-types and virally encoded miRNAs. Nucleic Acids Res. 2024;52(D1):D304-d10.

34. Ru Y, Kechris KJ, Tabakoff B, et al. The multiMiR R package and database: integration of microRNA-target interactions along with their disease and drug associations. Nucleic Acids Res. 2014;42(17):e133.

35. The Gene Ontology resource: enriching a GOld mine. Nucleic Acids Res. 2021;49(D1):D325-d34.

36. Kanehisa M, Goto S. KEGG: kyoto encyclopedia of genes and genomes. Nucleic Acids Res. 2000;28(1):27-30.

37. Yu G, Wang LG, Han Y, et al. clusterProfiler: an R package for comparing biological themes among gene clusters. Omics. 2012;16(5):284-7.

38. Glueck DH, Mandel J, Karimpour-Fard A, et al. Exact calculations of average power for the Benjamini-Hochberg procedure. Int J Biostat. 2008;4(1):Article 11.

39. Bindea G, Mlecnik B, Hackl H, et al. ClueGO: a Cytoscape plug-in to decipher functionally grouped gene ontology and pathway annotation networks. Bioinformatics. 2009;25(8):1091-3.

40. Kramer MF. Stem-loop RT-qPCR for miRNAs. Curr Protoc Mol Biol. 2011;Chapter 15:Unit 15.0.

41. Łukasiewicz S, Czeczelewski M, Forma A, et al. Breast Cancer-Epidemiology, Risk Factors, Classification, Prognostic Markers, and Current Treatment Strategies-An Updated Review. Cancers (Basel). 2021;13(17).

42. Lose F, Lovelock P, Chenevix-Trench G, et al. Variation in the RAD51 gene and familial breast cancer. Breast Cancer Res. 2006;8(3):R26.

43. Fischer JW, Leung AK. CircRNAs: a regulator of cellular stress. Crit Rev Biochem Mol Biol. 2017;52(2):220-33.

44. Hoque P, Romero B, Akins RE, et al. Exploring the Multifaceted Biologically Relevant Roles of circRNAs: From Regulation, Translation to Biomarkers. Cells. 2023;12(24).

45. Huang X, Song C, Zhang J, et al. Circular RNAs in breast cancer diagnosis, treatment and prognosis. Oncol Res. 2023;32(2):241-9.

46. Fu B, Liu W, Zhu C, et al. Circular RNA circBCBM1 promotes breast cancer brain metastasis by modulating miR-125a/BRD4 axis. Int J Biol Sci. 2021;17(12):3104-17.

47. Yin WB, Yan MG, Fang X, et al. Circulating circular RNA hsa_circ_0001785 acts as a diagnostic biomarker for breast cancer detection. Clin Chim Acta. 2018;487:363-8.

48. Allegra A, Cicero N, Tonacci A, et al. Circular RNA as a Novel Biomarker for Diagnosis and Prognosis and Potential Therapeutic Targets in Multiple Myeloma. Cancers (Basel). 2022;14(7).

49. Morovat P, Morovat S, Ashrafi AM, et al. Identification of potentially functional circular RNAs hsa_circ_0070934 and hsa_circ_0004315 as prognostic factors of hepatocellular carcinoma by integrated bioinformatics analysis. Scientific Reports. 2022;12(1):4933.

50. Zhao Y, Zhao Y, Liu L, et al. Tumor-exosomal miR-205-5p as a diagnostic biomarker for colorectal cancer. Clin Transl Oncol. 2025;27(3):1185-97.

51. De Cola A, Lamolinara A, Lanuti P, et al. MiR-205-5p inhibition by locked nucleic acids impairs metastatic potential of breast cancer cells. Cell Death Dis. 2018;9(8):821.

52. Li JH, Sun SS, Li N, et al. MiR-205 as a promising biomarker in the diagnosis and prognosis of lung cancer. Oncotarget. 2017;8(54):91938-49.

53. Cabrera M, Kolli M, Jaggi M, et al. miRNA-205: a future therapeutic molecule for liver diseases. Future Drug Discov. 2023;4(3):Fdd78.

54. Kalinkova L, Nikolaieva N, Smolkova B, et al. miR-205-5p Downregulation and ZEB1 Upregulation Characterize the Disseminated Tumor Cells in Patients with Invasive Ductal Breast Cancer. Int J Mol Sci. 2021;23(1):103.

55. Gulei D, Magdo L, Jurj A, et al. The silent healer: miR-205-5p up-regulation inhibits epithelial to mesenchymal transition in colon cancer cells by indirectly up-regulating E-cadherin expression. Cell Death Dis. 2018;9(2):66.

56. Fan Y, Wang K. miR-205 suppresses cell migration, invasion and EMT of colon cancer by targeting mouse double minute 4. Mol Med Rep. 2020;22(2):633-42.

57. Shao P, Qu WK, Wang CY, et al. MicroRNA-205-5p regulates the chemotherapeutic resistance of hepatocellular carcinoma cells by targeting PTEN/JNK/ANXA3 pathway. Am J Transl Res. 2017;9(9):4300-7.

58. Guo Z, Zhu H, Zhang R, et al. miR-205-5p Promotes the Proliferation, Migration, and Invasion of Nasopharyngeal Carcinoma Cells by Regulating CALM1. Crit Rev Immunol. 2025;45(2):25-38.

59. 53Xiao Y, Humphries B, Yang C, et al. MiR-205 Dysregulations in Breast Cancer: The Complexity and Opportunities. Noncoding RNA. 2019;5(4):53.

60. Klein HL. The consequences of Rad51 overexpression for normal and tumor cells. DNA Repair (Amst). 2008;7(5):686-93.

61. Babu S, Krishnan M, Chinnaiyan M, et al. MiR-205-5P AS POTENTIAL BIOMARKER AND THERAPEUTIC TARGET IN HEAD AND NECK SQUAMOUS CELL CARCINOMA. Exp Oncol. 2022;44(4):337-8.

62. Wang Z, Jia R, Wang L, et al. The Emerging Roles of Rad51 in Cancer and Its Potential as a Therapeutic Target. Front Oncol. 2022;12:935593.

63. So A, Dardillac E, Muhammad A, et al. RAD51 protects against nonconservative DNA double-strand break repair through a nonenzymatic function. Nucleic Acids Res. 2022;50(5):2651-66.

64. Cruz C, Castroviejo-Bermejo M, Gutiérrez-Enríquez S, et al. RAD51 foci as a functional biomarker of homologous recombination repair and PARP inhibitor resistance in germline BRCA-mutated breast cancer. Ann. Oncol. 2018;29(5):1203-10.

65. Ajith AK, Subramani S, Manickam AH, et al. Chemotherapeutic resistance genes of breast cancer patients-an overview. Adv. Pharm. Bull. 2021;12(4):649.

66. Wu R, Patel A, Tokumaru Y, et al. High RAD51 gene expression is associated with aggressive biology and with poor survival in breast cancer. Breast Cancer Res. Treat. 2022;193(1):49-63.

67. Liu YC, Shen J. Meta-analysis of the association between overexpression of RAD51 family genes and prognosis and clinical features in breast cancer. Sci Rep. 2025;15(1):4229.